Published for SISSA by Springer

Received: *January 20, 2023*
Revised: *August 16, 2023*
Accepted: *September 25, 2023*
Published: *October 4, 2023*

Enhancement of the screening effect in semiconductor detectors in the presence of the neutrino magnetic moment

Yu-Feng Li and Shuo-yu Xia[1]

Institute of High Energy Physics, Chinese Academy of Sciences, Beijing 100049, China
School of Physical Sciences, University of Chinese Academy of Sciences, Beijing 100049, China

E-mail: liyufeng@ihep.ac.cn, xiashuoyu@ihep.ac.cn

Abstract: The theoretical framework of the neutrino electron excitation at low energies including the screening effect in semiconductor detectors is developed for the first time, both in the Standard Model of particle physics and in the presence of the neutrino magnetic moment. We apply the framework of the non-relativistic effective theory on the neutrino electron scattering and explore the contribution of the screening effect of semiconductors to the neutrino electron excitation based on the linear response theory. We calculate the corresponding numerical results with the popular silicon and germanium targets and show that excitation rates from the neutrino magnetic moment are dramatically enhanced by the screening effect and the sensitivity can be significantly improved to the level of $10^{-13}\,\mu_B$, much better than the current best limits from the laboratory and astrophysical probes.

Keywords: Neutrino Interactions, Non-Standard Neutrino Properties

ArXiv ePrint: 2211.11582

[1]Corresponding author.

Open Access, © The Authors.
Article funded by SCOAP[3].

https://doi.org/10.1007/JHEP10(2023)021

JHEP10(2023)021

Contents

1 Introduction

Neutrino interaction [1] is one of the most important ingredients of the neutrino observation, among which the elastic neutrino electron scattering process has been widely used in the detection of solar neutrinos [2–4], reactor neutrinos [5–7] and accelerator neutrinos [8, 9], and played important roles in studying fundamental properties of neutrino oscillations and new physics beyond the Standard Model (SM). For the state-of-the-art semiconductor dark matter (DM) detectors, such as SENSEI [10], EDELWEISS [11] and SuperCDMS [12], the sensitivity has reached sub-keV and the collective behaviors of electrons can make important contributions to the relative electron excitations, which are neglected in most of the present applications.

As a fundamental property of massive neutrinos, the magnetic moment is estimated to be vanishingly small in simple extensions of SM [13, 14]. However, the neutrino magnetic moment can be significantly enhanced in many models beyond the simplest SM extension [15, 16], and even can reach the testable level of the current limits from laboratory measurements [5–7, 14] and astrophysical considerations [17–20]. Note that the recent results from XENONnT have pushed the laboratory limit down to $6.4 \times 10^{-12}\mu_{\rm B}$ at the 90% confidence level [21]. Since the contribution of the neutrino magnetic moment to the neutrino electron excitation rate is enhanced by the inverse of the recoil energy, semiconductor detectors take significant advantages compared to other popular detectors for a lower energy threshold.

The thresholds of present semiconductor detectors are already capable of going even below 0.1 keV, where the conventional scattering theory with non-interacting particle states cannot precisely describe the related physics. The collective behaviors of electrons at such low energies in semiconductor detectors, which have attracted various attentions in the fields of DM direct detection [22–27], play an important role in such scenarios. The

JHEP10(2023)021

related underlying physics including the screening effect can be well described with the dielectric function of the material and the in-medium effects of the DM-electron excitation are thoroughly investigated in refs. [28, 29].

The theory to describe the in-medium screening effect for DM-electron scattering in crystal have already been developed in ref. [30]. The energy loss function (ELF), which is defined as the imaginary part of the inverse dielectric function in the homogeneous electron gas (HEG), describes the rate for particles to loss the momentum and energy when passing through the material and it is the key to describe the DM-electron excitation. To generalize the results of HEG to the isotropic crystal target, an effective form of the inverse dielectric function is taken as the average of the diagonal elements of the general matrix of the inverse dielectric function. Moreover, the linear response theory is employed to describe the screened DM-electron scattering as a perturbation exerted onto the electron system.

The purpose of this work is to develop for the first time the general theory of the neutrino-electron excitation in isotropic semiconductors including the screening effect, since previous calculations from the conventional scattering theory have underestimated some important features of the electron response under low energies. We generalize the non-relativistic effective filed theory framework (NR EFT) in ref. [31] to the neutrino-electron couplings in order to study the effective Lagrangian applied in the non-relativistic neutrino-electron excitation. In order to illustrate the enhanced response in the contribution of the neutrino magnetic moment, we calculate the constraints from semiconductor detectors using the solar neutrinos, whose sensitivity approaches the level of $10^{-13}\,\mu_{\rm B}$, much better than the current best limit from laboratory and astrophysical probes.

2 Neutrino couplings to non-relativistic electrons

The elastic neutrino electron scattering (EνES) can be described with the following standard Lagrangian

$$\mathcal{L}_{\rm E\nu ES} = -i\frac{G_F}{\sqrt{2}}\left[\bar{\nu}_\alpha\gamma^\rho(1-\gamma^5)\nu_\alpha\right]\left[\bar{\phi}_e\gamma_\rho(g_{\alpha;\rm V}-g_{\alpha;\rm A}\gamma^5)\phi_e\right], \tag{2.1}$$

where $g_{e;\rm V} = 1/2 + 2\sin^2\theta_W$, $g_{e;\rm A} = 1/2$ for the electron neutrino and $g_{\mu,\tau;\rm V} = -1/2 + 2\sin^2\theta_W$, $g_{\mu,\tau;\rm A} = -1/2$ for muon and tau neutrinos. $L^\rho = \bar{\nu}_\alpha\gamma^\rho(1-\gamma^5)\nu_\alpha$ denotes the neutrino current and this structure will be kept unchanged in the following calculation until we deal with the square of the scattering amplitude. Since the scattering process we have focused in this work occurs at very low energies, it is reasonable to employ the approximation that the momentum of electrons can be neglected compared to the electron mass and so is the momentum transfer compared to the neutrino energy. Meanwhile, we make the assumption that the semiconductor crystal is isotropic as in most popular detectors with these mediums. Under the above assumption, the neutrino current L^ρ can be written as the respective temporal and spatial components

$$\begin{aligned}
&\overline{u}^r_\alpha(\boldsymbol{k}_1)\gamma^0(1-\gamma^5)u^r_\alpha(\boldsymbol{p}_1) \approx 2E_\nu - 2rE_\nu,\\
&\overline{u}^r_\alpha(\boldsymbol{k}_1)\gamma^i(1-\gamma^5)u^r_\alpha(\boldsymbol{p}_1) \approx -2E_\nu\frac{1}{r}.
\end{aligned} \tag{2.2}$$

JHEP10(2023)021

The spatial part of the neutrino current are approximately cancelled due to the spin summation in the amplitude calculation and only the temporal part contributes to the scattering process at the leading order. Then the Lagrangian of EνES can be written as the vector and axial-vector parts

$$\mathcal{L}_{\mathrm{E}\nu\mathrm{ES}} = -i\frac{G_F}{\sqrt{2}} g_{\alpha;\mathrm{V}} L^0 \bar{\phi}_e \gamma_0 \phi_e + i\frac{G_F}{\sqrt{2}} g_{\alpha;\mathrm{A}} L^0 \bar{\phi}_e \gamma_0 \gamma^5 \phi_e + [\boldsymbol{L}]\,, \tag{2.3}$$

where the terms of spatial components are included in $[\boldsymbol{L}]$ and will not be considered at the leading order calculation. In the energy range we are concerned in this work, NR EFT is a reasonable approximation [32, 33] to describe the neutrino-electron interaction. To match the relativistic theory of EνES onto the framework of the NR EFT with effective operators, we employ the techniques from ref. [31] and obtain the leading order non-relativistic Lagrangian of EνES as

$$\mathcal{L}_{\mathrm{E}\nu\mathrm{ES}} = -i\sqrt{2} G_{\mathrm{F}} g_{\alpha;\mathrm{V}} \bar{\nu}_{\alpha,L} \gamma^0 \nu_{\alpha,L} \phi_+^\dagger \phi_+\,, \tag{2.4}$$

where $V_{\mathrm{E}\nu\mathrm{ES}} = -i\sqrt{2} G_F g_{\alpha;\mathrm{V}}$, is defined as the effective non-relativistic potential of EνES, ϕ_+ is the non-relativistic effective operator of the electron field, and its definition can be found in eq. (A.2) of appendix A. Note that this non-relativistic Lagrangian is vector dominant. A detailed calculation of the non-relativistic Lagrangian in eq. (2.4) is provided in appendix A.

The scattering process between a electron and a neutrino in the presence of the neutrino magnetic moment can be described with the Lagrangian

$$\mathcal{L}_{\mathrm{mag}} = -i\mu_\nu \frac{m_\nu}{m_e} \frac{4\pi\alpha}{q^2} \left[\bar{\nu}_\alpha (1-\gamma^5) i \frac{\sigma^{\mu\nu} q_\nu}{2m_\nu} \nu_\alpha\right] \left[\bar{\phi}_e \gamma_\mu \phi_e\right]\,, \tag{2.5}$$

with m_ν and m_e being masses of the neutrino and electron respectively and μ_ν being the neutrino magnetic moment. With the Gordon Identity, the above Lagrangian can be separated into two terms

$$\begin{aligned} \mathcal{L}_{\mathrm{mag}} = &-i\mu_\nu \frac{m_\nu}{m_e} \frac{4\pi\alpha}{q^2} \left[\bar{\nu}_\alpha \gamma^\mu (1-\gamma^5) \nu_\alpha\right] \left[\bar{\phi}_e \gamma_\mu \phi_e\right] \\ &+ i\mu_\nu \frac{1}{2m_e} \frac{4\pi\alpha}{q^2} \left[\bar{\nu}_\alpha (1-\gamma^5)(p_1+k_1)^\mu \nu_\alpha\right] \left[\bar{\phi}_e \gamma_\mu \phi_e\right]\,, \end{aligned} \tag{2.6}$$

where p_1 and k_1 are the four momenta of the initial and final neutrinos respectively. In this work the neutrino mass is less than 1 eV and the first term will not be considered in the following leading order calculation. Thus the Lagrangian can be written as

$$\begin{aligned} \mathcal{L}_{\mathrm{mag}} &= i\mu_\nu \frac{1}{2m_e} \frac{4\pi\alpha}{q^2} \left[\bar{\nu}_\alpha (1-\gamma^5) 2p_1^\mu \nu_\alpha\right] \left[\bar{\phi}_e \gamma_\mu \phi_e\right] \\ &\quad - i\mu_\nu \frac{1}{2m_e} \frac{4\pi\alpha}{q^2} \left[\bar{\nu}_\alpha (1-\gamma^5) q^\mu \nu_\alpha\right] \left[\bar{\phi}_e \gamma_\mu \phi_e\right] + \mathcal{O}\left[\frac{m_\nu}{m_e}\right] \\ &= i\mu_\nu \frac{1}{2m_e} \frac{4\pi\alpha}{q^2} \left[\bar{\nu}_\alpha (1-\gamma^5) 2p_1^\mu \nu_\alpha\right] \left[\bar{\phi}_e \gamma_\mu \phi_e\right] + \mathcal{L}_{\mathrm{cor}}(q) + \mathcal{O}\left[\frac{m_\nu}{m_e}\right]\,, \end{aligned} \tag{2.7}$$

where q is the transferred momentum and we refer the term with transferred momentum q as $\mathcal{L}_{\mathrm{cor}}(q)$. Since the transferred momentum q is much less than the neutrino momentum

JHEP10(2023)021

in the process we are interested about, the initial and final state of the neutrino can be approximately treated as unchanged at the leading order. Therefore, the term $\mathcal{L}_{\rm cor}(q)$ is the only term left that encode the kinematic correlation between the neutrino and electron. However, this term will not take effect at the leading order since it is proportional to the transferred momentum q. Then we can write the first term of eq. (2.7) in two terms of temporal and spatial components of the initial neutrino momentum respectively

$$\begin{aligned}\mathcal{L}_{\rm mag} = & i\mu_\nu \frac{1}{2m_e}\frac{8\pi\alpha}{q^2}\left[\bar{\nu}_\alpha(1-\gamma^5)p_1^0\nu_\alpha\right]\left[\bar{\phi}_e\gamma_0\phi_e\right] + i\mu_\nu \frac{1}{2m_e}\frac{8\pi\alpha}{q^2}\left[\bar{\nu}_\alpha(1-\gamma^5)p_1^i\nu_\alpha\right]\left[\bar{\phi}_e\gamma_i\phi_e\right] \\ & - \mathcal{L}_{\rm cor}(q) + \mathcal{O}\left[\frac{m_\nu}{m_e}\right], \end{aligned} \tag{2.8}$$

Because of the lack of the kinematic correlation between the spatial term of the neutrino current $\bar{\nu}_\alpha(1-\gamma^5)p_1^i\nu_\alpha$ and the corresponding electron current $\bar{\phi}_e\gamma_i\phi_e$, they can be treated separately in the summation of crystal cells in next section. Due to the isotropic structure of the crystal, a directional neutrino flux can be considered as isotropic for the whole target that contains cells of $\mathcal{O}(10^{23})$ after all the cells are turned to the same direction. As a result, the spatial term of the neutrino current will be integrated out as zero for the isotropic crystal after the summation of crystal cells. Therefore, the whole spatial term will not affect the final results in the isotropic crystal. Then the effective Lagrangian to describe the contribution of the neutrino magnetic moment at leading order in the isotropic crystal can be written with only the temporal component of the first term in eq. (2.8)

$$\mathcal{L}_{\rm mag} = i\mu_\nu \frac{E_\nu}{m_e}\frac{8\pi\alpha}{q^2}\left[\bar{\nu}_{\alpha,L}\nu_{\alpha,L}\right]\left[\bar{\phi}_e\gamma_0\phi_e\right]. \tag{2.9}$$

The structure of the leading order Lagrangian is the same as the vector part of the standard EνES Lagrangian and it can be written in a similar way as in appendix A with the non-relativistic effective Lagrangian

$$\mathcal{L}_{\rm mag} = i\mu_\nu \frac{E_\nu}{m_e}\frac{8\pi\alpha}{q^2}\bar{\nu}_{\alpha,\rm L}\nu_{\alpha,\rm L}\phi_+^\dagger\phi_+ = V_{\nu,\rm mag}(\boldsymbol{q})\bar{\nu}_{\alpha,\rm L}\nu_{\alpha,\rm L}\phi_+^\dagger\phi_+ , \tag{2.10}$$

where $V_{\nu,\rm mag}(\boldsymbol{q})$ is similarly defined as the effective potential of the contribution of the neutrino magnetic moment.

3 EνES in crystalline solids

As mentioned above, to describe the scattering process in the crystal in the context of the linear response theory, it is convenient to regard the effects of the incident particle as a perturbation on the electron system [30]. For the case of electron energy loss spectroscopy (EELS) in the HEG, the effects of incident electron can be described with the following effective Hamiltonian with the Coulomb potential $V_{\rm cou}(\boldsymbol{Q})$

$$\hat{H}_I(t) = V_{\rm cou}(\boldsymbol{Q})\int e^{i\boldsymbol{Q}\cdot\boldsymbol{x}}\hat{\rho}_I(\boldsymbol{x},t)e^{i\omega_{p'p}t}\,\mathrm{d}^3x\,, \tag{3.1}$$

JHEP10(2023)021

where $\hat{\rho}_I(\boldsymbol{x},t)$ is the density operator of the electron and $\omega_{p'p} = E'_e - E_e$ is the energy difference of the electron. As in ref. [30], the averaging and spin summing calculation can be related to a correlation function

$$S^{\hat{H}_I^\dagger \hat{H}_I}(-\omega_{p'p}) = \sum_{i,f} p_i \left| < f|\hat{H}_I|i > \right|^2 (2\pi)\delta(\epsilon_f - \epsilon_i + \omega_{p'p})\,, \tag{3.2}$$

where p_i is the thermal distribution of the initial state $|i>$. Using the fluctuation-dissipation theorem, the correlation function $S^{\hat{H}_I^\dagger \hat{H}_I}(\omega)$ can be expressed with the zero-temperature approximation as

$$S^{\hat{H}_I^\dagger \hat{H}_I}(\omega) = 2V\,|V_{\rm cou}(\boldsymbol{Q})|\,{\rm Im}\left[\frac{-1}{\epsilon({\rm Q},\omega)}\right] \tag{3.3}$$

with $\epsilon(\boldsymbol{Q},\omega)$ being the dielectric function and V being the material volume. It should be noticed that the structure of the electron part in eq. (2.4) is the same with that in the Coulomb interaction and the neutrino part will be calculated with the averaging and spin summing as in the relativistic theory due to the relativistic property of neutrinos. Therefore, to calculate the cross section of EνES with this technique, we replace the Coulomb potential with the effective potential of EνES in eq. (2.4) and the correlation function $S^{\hat{H}_I^\dagger \hat{H}_I}(\omega)$ can be expressed as

$$S^{\hat{H}_I^\dagger \hat{H}_I}(\omega) = 2V\frac{|V_{\rm E\nu ES}|^2}{|V_{\rm cou}(\boldsymbol{Q})|}{\rm Im}\left[\frac{-1}{\epsilon({\rm Q},\omega)}\right] \tag{3.4}$$

According to the above discussion, one can obtain the cross section for EνES in the HEG by inserting the correlation function as

$$\sigma = -\frac{\Omega G_F^2 g_{\alpha;{\rm V}}^2}{\pi\alpha}\int\frac{{\rm d}^3Q}{(2\pi)^3}\boldsymbol{Q}^2{\rm Im}\left[\frac{-1}{\epsilon({\rm Q},\omega)}\right]\delta(\omega+\omega_{\rm p'p})\,{\rm d}\omega\,. \tag{3.5}$$

This cross section describes the response of the zero-temperature electron gas induced by an incident electron, which will lead to the collective oscillations of electron gas, and can be treated as the quasiparticle known as the plasmon. From the viewpoint of quantum field theory, the plasmon contributes to the renormalized interaction which takes into account all of the graphs that includes additional loops in the form of a phonon-like propagator. This propagator leads to a pole in the frequency-dependent Green's function and correspond to a quasiparticle [34]. At the higher transferred momentum of $\boldsymbol{Q}$ the plasmon energy can be lost to free electrons, which is known as the Landau damping effect, and the plasmon have a large decay width with this process. However, at lower transferred momenta, this is not dynamically allowed and thus a peak is created in the ELF at the position of the pole. As a result, the ELF has a plasmon peak at the low transferred momentum that significantly increases the response rate at the corresponding energy and the peak is smoothed as the transferred momentum increases.

In a crystalline solid, the correlation function is expressed in the reciprocal space periodically and connected to the microscopic dielectric matrix due to the translational symmetry of the crystal lattice. As a result, the transferred momentum $\boldsymbol{Q}$ can be split

JHEP10(2023)021

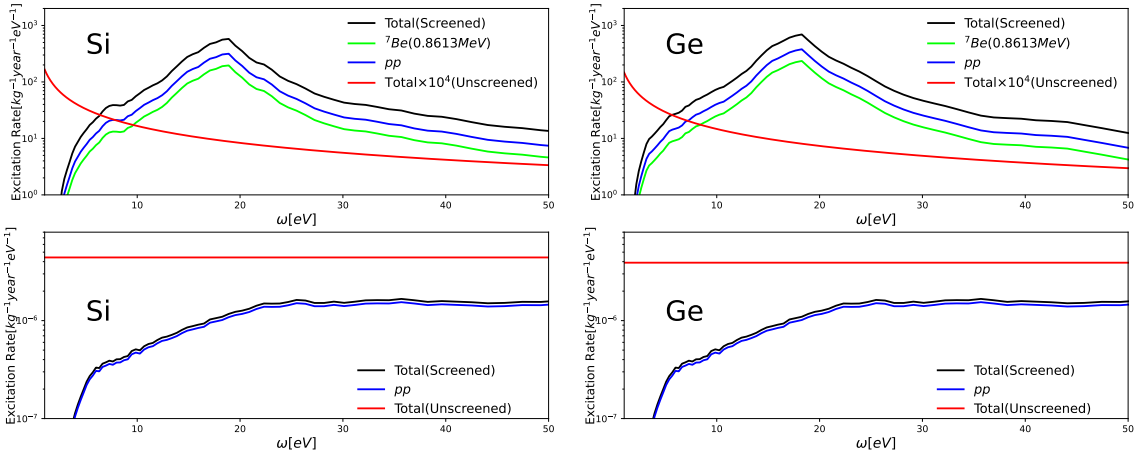

Figure 1. The differential excitation rate in silicon (left) and germanium (right) target induced by solar neutrino with the neutrino magnetic moment $\mu_\nu = 10^{-11}\mu_B$ (Top) and in the SM (Bottom). We show the total excitation rate with screening effect with black line and unscreened results calculated from the independent particle EνES process without the screening effects in red line. The main excitation rate comes from the *pp* neutrino (blue lines). We also show the excitation rate from the ^{7}Be neutrino with the peak at 0.8613 MeV in the presence of the neutrino magnetic moment, which induces the second largest contribution in this case.

into a reduced momentum $\boldsymbol{q}$ in 1 Brillouin Zone (BZ) and a reciprocal momentum $\boldsymbol{G}$. Therefore, with above discussion, the cross section of EνES for the HEG in eq. (3.5) can be extended to the case in the crystalline solid as

$$\sigma = \frac{\Omega G_F^2 g_{\alpha;\mathrm{V}}^2}{\pi\alpha} \sum_G \int_{1\mathrm{BZ}} \frac{\mathrm{d}^3 q}{(2\pi)^3} |\boldsymbol{G}+\boldsymbol{q}|^2 \times \mathrm{Im}\left[\frac{1}{\epsilon_{\mathrm{G,G}}(\mathrm{q},\omega)}\right] \delta(\omega+\omega_{\mathrm{p'p}})\,\mathrm{d}\omega\,, \tag{3.6}$$

where Ω is the volume of a cell of the target crystal. In above calculation, we take the local field effects into consideration and express the microscopic dielectric matrix element $\mathrm{Im}[-\epsilon^{-1}_{\boldsymbol{G},\boldsymbol{G}'}(\boldsymbol{q},\omega)]$ approximately as its diagonal components $\mathrm{Im}[-\epsilon^{-1}_{\boldsymbol{G},\boldsymbol{G}}(\boldsymbol{q},\omega)]$, which is averaged over $\boldsymbol{q}$ and $\boldsymbol{G}$. For a target with N_{cell} crystal cells exposed to a neutrino flux $\Phi(E_\nu)$, the excitation rate can be written as

$$\begin{aligned} R = \frac{N_{\mathrm{cell}}\Omega G_F^2 g_{\alpha;\mathrm{V}}^2}{\pi\alpha} \int \Phi(E_\nu)\,\mathrm{d}E_\nu \sum_G \int_{1\mathrm{BZ}} \frac{\mathrm{d}^3 q\,\mathrm{d}\omega}{(2\pi)^3} \\ \times |\boldsymbol{G}+\boldsymbol{q}|^2\,\mathrm{Im}\left[\frac{1}{\epsilon_{\mathrm{G,G}}(\mathrm{q},\omega)}\right] \delta(\omega+\omega_{\mathrm{p'p}})\,\mathrm{d}\cos\theta_{\mathrm{p,Q}} \end{aligned} \tag{3.7}$$

In this work we assume an isotropic crystal target and it is a straight forward exercise to integrate out the δ function in terms of Heaviside function Θ as

$$\begin{aligned} \int_{-1}^{1} \delta(\omega+\omega_{p'p})\,\mathrm{d}\cos\theta_{\boldsymbol{p},\boldsymbol{Q}} \simeq \frac{1}{|\boldsymbol{G}+\boldsymbol{q}|}[\Theta(|\boldsymbol{G}+\boldsymbol{q}|-\omega)\Theta(E_\nu-|\boldsymbol{G}+\boldsymbol{q}|) \\ + \Theta(2E_\nu-|\boldsymbol{G}+\boldsymbol{q}|-\omega)\Theta(|\boldsymbol{G}+\boldsymbol{q}|-E_\nu)]\,. \end{aligned} \tag{3.8}$$

JHEP10(2023)021

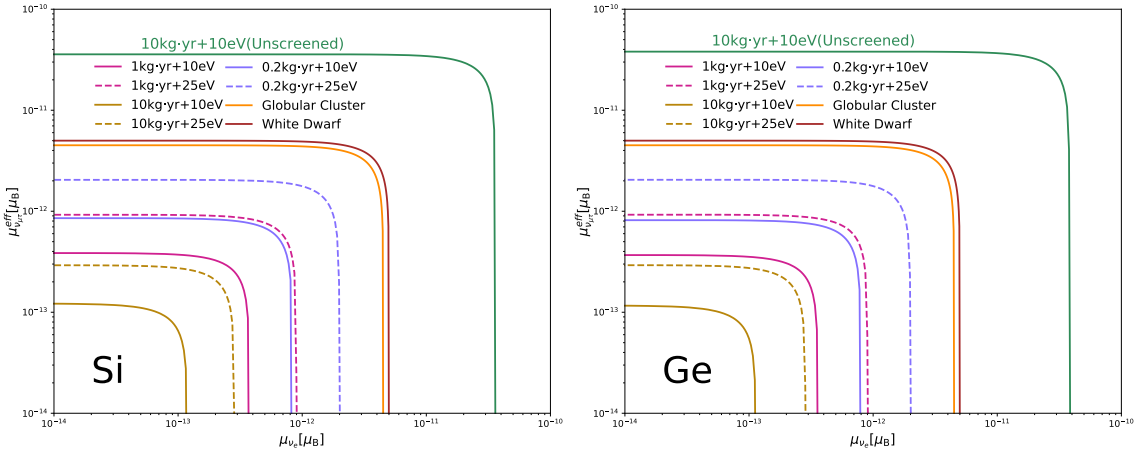

Figure 2. Constraints for the neutrino magnetic moments with screening effect under 50 eV at 90% confidence level based on silicon (left) and germanium (right) experiment sets of different target mass and threshold. We also show the constraints without screening effect based on 10 kg target and 10 eV threshold. We employ a flat background of 100 $\mathrm{keV}^{-1}\mathrm{t}^{-1}\mathrm{yr}^{-1}$ and an ideal efficiency of 100% and set the experiment time to be one year. We also show the constraints from the astrophysical observation of the globular cluster M5 [17] and the white dwarf [18].

With the above relation, the excitation rate in eq. (3.7) can be written in terms of the transferred momentum $|\boldsymbol{G}+\boldsymbol{q}|$ and the dielectric matrix element $\epsilon_{\boldsymbol{G},\boldsymbol{G}}(\boldsymbol{q},\omega)$ with a more clear structure

$$R = \frac{N_{\mathrm{cell}}\Omega G_F^2 g_{\alpha;\mathrm{V}}^2}{\pi\alpha}\int \Phi(E_\nu)\,\mathrm{d}E_\nu \times \sum_G \int_{1\mathrm{BZ}} \frac{\mathrm{d}^3q\,\mathrm{d}\omega}{(2\pi)^3}\,|\boldsymbol{G}+\boldsymbol{q}|\,\mathrm{Im}\left[\frac{1}{\epsilon_{\mathrm{G,G}}(\mathrm{q},\omega)}\right] \tag{3.9}$$
$$\times\left[\Theta(|\boldsymbol{G}+\boldsymbol{q}|-\omega)\Theta(E_\nu-|\boldsymbol{G}+\boldsymbol{q}|)+\Theta(2E_\nu-|\boldsymbol{G}+\boldsymbol{q}|-\omega)\Theta(|\boldsymbol{G}+\boldsymbol{q}|-E_\nu)\right].$$

It should be noticed that the above expression includes the momentum transfer term $|\boldsymbol{G}+\boldsymbol{q}|$, which will enhance the response of the target crystal at high values of the momentum transfer.

For the contribution of the neutrino magnetic moment, we can obtain the excitation rate in a similar way after replacing the effective potential with $V_{\nu,\mathrm{mag}}$ in eq. (2.10)

$$R = 32N_{\mathrm{cell}}\Omega\mu_\nu^2\frac{\pi\alpha}{m_e^2}\int \Phi(E_\nu)E_\nu^2\,\mathrm{d}E_\nu \times \sum_G \int_{1\mathrm{BZ}} \frac{\mathrm{d}^3q\,\mathrm{d}\omega}{(2\pi)^3}\frac{1}{|\boldsymbol{G}+\boldsymbol{q}|^3}\mathrm{Im}\left[\frac{1}{\epsilon_{\mathrm{G,G}}(\mathrm{q},\omega)}\right] \tag{3.10}$$
$$\times\left[\Theta(|\boldsymbol{G}+\boldsymbol{q}|-\omega)\Theta(E_\nu-|\boldsymbol{G}+\boldsymbol{q}|)+\Theta(2E_\nu-|\boldsymbol{G}+\boldsymbol{q}|-\omega)\Theta(|\boldsymbol{G}+\boldsymbol{q}|-E_\nu)\right]$$

In this case, the excitation rate includes the momentum transfer term $1/|\boldsymbol{G}+\boldsymbol{q}|^3$ that will significantly enhance the response of target at lower values of the momentum transfer, which would help us to improve the limit on the neutrino magnetic moment.

4 Constraints on the neutrino magnetic moment

In this work, we choose germanium and silicon, which are the most popular materials for the semiconductor detectors of DM direct detection, as the target materials of this

JHEP10(2023)021

work and employ the corresponding dielectric function calculated with the time-dependent density function theory in refs. [35, 36].

In figure 1, we show the differential excitation rates of the EνES induced by solar neutrinos with (upper panels) and without (lower panels) the neutrino magnetic moment. In this work we employ the solar neutrino fluxes from the standard solar model BS05(OP) [37–39]. The left and right panels are for the materials of germanium and silicon respectively. Here solar neutrinos are used for illustration since they are the most intensive natural neutrino source on the Earth. In the upper panels, we show the differential excitation rates with $\mu_\nu = 10^{-11}\mu_{\rm B}$, which is similar to the current limits from the LUX-ZEPLIN [40] and XENON [21, 41] experiments. The unscreened results are calculated from the independent particle EνES process without the screening effects and shown in red lines. They are dominated by the term that inversely proportions to the recoil energy. With the dominant contribution from *pp* and ^{7}Be neutrinos, the screened results of the black lines show a significant peak induced by the plasmon from the material response. As mentioned above, the term $1/|\boldsymbol{G}+\boldsymbol{q}|^3$ from the contribution of the neutrino magnetic moment dramatically enhances the response of the electron at lower values of the momentum transfer, where the plasmon peak is much more significant since the plasmon is long-lived in this range [23].

In the bottom panels, we show the differential excitation rates in the SM. The screened results, which are significantly lower, heavily rely on the electron response and is dominated by *pp* neutrinos even more than that with the neutrino magnetic moment. Below 5 eV there is nearly no observable response and so is the excitation rate. There is no peak in this case since the $|\boldsymbol{G}+\boldsymbol{q}|$ term in eq. (3.9) enhances the response at high momentum transfer, where the plasmon peak is also not significant because the plasmon has a large decay width in this range for its dispersion matching into kinematically-accessible single electron-hole excitations [23].

To explore the projected constraints of different targets on the neutrino magnetic moments with and without the screening effect, we employ the standard least squares method

$$\chi^2 = \sum_{i=1}^{n}\left(\frac{N_i^{\rm exp} - (1+\epsilon_{\rm exp})N_i^{\rm pred}[(1+\epsilon_j)\Phi_{\rm SSM}^j]}{\sigma_i}\right)^2 + \left(\frac{\epsilon_{\rm exp}}{\sigma_{\rm exp}}\right)^2 + \Sigma_j\left(\frac{\epsilon_j}{\sigma_{\Phi_{\rm SSM}^j}}\right)^2, \quad (4.1)$$

where $\sigma_i^2 = N_i^{\rm exp}$, $N_i^{\rm exp}$ is the pseudo event number of the signal of the considered experiment in the ith energy bin, $N_i^{\rm pred}$ is the predicted event number. $\epsilon_{\rm exp}$ is the simplified nuisance parameter which quantifies the total detection uncertainty of the experiment and $\sigma_{\rm exp} = 5\%$ is the corresponding standard deviation we expected. ϵ_j and $\sigma_{\Phi_{\rm SSM}^j}$ are the nuisance parameter and uncertainty of the jth solar neutrino flux from the SSM, in which the largest one is 11.6% for the ^{8}B neutrino flux. Since the background study at such low energy is lacking, we employ a flat background of 100 keV^{-1}t^{-1}yr^{-1} based on the discussion of SuperCDMS in ref. [42]. Nowadays semiconductor detectors have already achieved a high efficiency for ionization signals and it is a convenient approximation to employ an ideal efficiency of 100% for illustration.

In figure 2 we illustrate the constraints on the neutrino magnetic moment including the screening effect for different detector setups, with μ_{ν_e} being the electron neutrino

JHEP10(2023)021

magnetic moment and $\mu^{\rm eff}_{\nu_{\mu\tau}} \simeq \sqrt{0.49\mu^2_{\nu_\mu} + 0.51\mu^2_{\nu_\tau}}$ being the effective parameter for μ and τ neutrinos [43]. We show the results based on different exposures of 10 kg·yr, 1 kg·yr and 0.2 kg·yr at 90% confidence level with two thresholds of 10 eV and 25 eV. The first two exposures are based on reasonable predictions of the experiments in the future decade and the last exposure of 0.2 kg·yr is based on the EDELWEISS experiment [44]. The two different thresholds enable the results to either include or exclude the plasmon peak. From the figure, one can find that a 10 eV threshold capable of detecting the plasmon effects would dramatically improve the sensitivity. We also note that increasing the exposure from 0.2 kg·yr to 1 kg·yr will improve the sensitivity by a factor of 2 and increasing the exposure from 1 kg·yr to 10 kg·yr will also improve the sensitivity by a factor of 3. Finally one would achieve an unprecedented sensitivity of $1 \times 10^{-13}\mu_{\rm B}$ using a near future semiconductor detectors with the screening effect, which is much better than the constraints from the astrophysical observation of the globular cluster M5 [17] and the white dwarf [18]. Even with a semiconductor detector of 0.2 kg·yr exposure and 10 eV threshold, which is similar to present ones like EDELWEISS [44], one can still achieve a sensitivity of $8 \times 10^{-13}\mu_{\rm B}$ and it is also better than the astrophysical constraints. Note that the sensitivity without the screening effect is at the level of $4 \times 10^{-11}\mu_{\rm B}$ even with 10 kg·yr and the 10 eV energy threshold and it can be concluded that the screening effects make significant contributions to the constraints of the neutrino magnetic moments.

5 Conclusion

In this work, we have developed for the first time the theoretical description of the neutrino electron excitation at low energies in semiconductors including the screening effect based on the fluctuation dissipation theorem, both within the SM and in the presence of the neutrino magnetic moment. We have shown that the excitation behaviors of the EνES process in semiconductor detectors are significantly altered because of the screening effect, and the excitation rates from the neutrino magnetic moment can be dramatically enhanced. The sensitivity on the neutrino magnetic moment can be significantly improved to the level of $10^{-13}\,\mu_{\rm B}$, which is much better than the current limits from laboratory and astrophysical probes, and would be important for the search for new physics beyond the SM.

Acknowledgments

The authors are very grateful to Zhengliang Liang for helpful discussions on the screening effect and the relative models. This work was supported in part by National Natural Science Foundation of China under Grant Nos. 12075255, 12075254 and 11835013, by the Key Research Program of the Chinese Academy of Sciences under Grant No. XDPB15.

A Application of non-relativistic effect field theory

In this appendix, we provide a detailed application of the NR EFT framework from ref. [31] on the EνES process in the SM. The case in the presence of the neutrino magnetic moment can be calculated in a similar way.

JHEP10(2023)021

To begin with, apart from the coupling to incident neutrinos, the electrons in semiconductors also couple to the background electromagnetic (EM) field, which can be described with the SM Lagrangian

$$\mathcal{L}_{\rm EM} = \bar{\phi}_e[i\gamma^\mu(\partial_\mu + ieA_\mu) - m_e]\phi_e\,. \tag{A.1}$$

In the NR EFT framework, the electron fields can be written in the effective operators

$$\phi_\pm(\boldsymbol{x}, t) = e^{-im_e t} P_\pm \phi_{\rm NR}(\boldsymbol{x}, t)\,, \tag{A.2}$$

where $P_\pm \equiv (1 \pm \gamma^0)/2$ is the projection operators and $\phi_{\rm NR}$ is the electron field in the non-relativistic theory. With the effective operator $\phi_\pm$, the SM Lagrangian can be written as

$$\begin{aligned}\mathcal{L}_{\rm EM} = {}& \phi_+^\dagger(i\partial_t - eA_0)\phi_+ + \phi_-^\dagger(i\partial_t - eA_0 + 2m_e)\phi_- \\ & + \phi_+^\dagger i\boldsymbol{\gamma}\cdot(\boldsymbol{\nabla} - ie\boldsymbol{A})\phi_- - \phi_-^\dagger i\boldsymbol{\gamma}\cdot(\boldsymbol{\nabla} - ie\boldsymbol{A})\phi_+\,.\end{aligned} \tag{A.3}$$

In this case, the photon field consists of a electrostatic background $A_{\rm bg}$ and a quantum fluctuation $\mathcal{A}^\mu$

$$\begin{aligned}A_0(\boldsymbol{x}, t) &= A_{\rm bg}(\boldsymbol{x}) + \mathcal{A}_0(\boldsymbol{x}, t)\,, \\ \boldsymbol{A}(\boldsymbol{x}, t) &= \boldsymbol{\mathcal{A}}(\boldsymbol{x}, t)\,,\end{aligned} \tag{A.4}$$

After separating the electrostatic background and quantum fluctuation components, we can integrate out the heavy field ϕ_- with the equation of motion and expand terms including ∇^2 with the non-relativistic Schrödinger equation at the leading order, which is already illustrated in detail in ref. [31]. Then we have

$$\mathcal{L}^{\rm eff}_{{\rm EM},\mathcal{A}} = -e\mathcal{A}\phi_+^\dagger\phi_+ - \frac{ie}{2m_e}\boldsymbol{\mathcal{A}}(\phi_+^\dagger \overleftrightarrow{\boldsymbol{\nabla}} \phi_+) + \frac{e}{2m_e}(\boldsymbol{\nabla}\times\boldsymbol{\mathcal{A}})\cdot(\phi_+^\dagger\boldsymbol{\Sigma}\phi_+) - \frac{e^2}{2m_e}\boldsymbol{\mathcal{A}}^2\phi_+^\dagger\phi_+\,. \tag{A.5}$$

The Lagrangian for EνES at low energies in eq. (2.3) includes both vector and axial-vector terms and we need to match onto the NR EFT framework in different ways due to their different Lorentz structures. To include the vector contribution of the EνES Lagrangian with a background electromagnetic field, we make the following replacement

$$e\mathcal{A}^\mu \to e\mathcal{A}^\mu - \frac{G_{\rm F}}{\sqrt{2}} g_{\alpha;{\rm V}} L^0\,. \tag{A.6}$$

Then after a similar calculation we obtain the effective Lagrangian for EνES with the contribution of the background electromagnetic field subtracted

$$\mathcal{L}^{\rm eff}_{{\rm E}\nu{\rm ES},{\rm V}} = -i\sqrt{2}G_{\rm F} g_{\alpha;{\rm V}}\bar{\nu}_{\alpha,L}\gamma^0\nu_{\alpha,L}\phi_+^\dagger\phi_+\,. \tag{A.7}$$

For the axial vector part, since there is no such structure in the electromagnetic part, we need to include such structure into the equation of motion. However, it is reasonable to substitute the equation of motion in this case with that of eq. (A.3) and integrate ϕ_- out in a similar way as the vector case since we only consider the terms at the leading order [31]. Therefore we can obtain the leading order Lagrangian as

$$\mathcal{L}^{\rm eff}_{{\rm E}\nu{\rm ES},{\rm A}} = -i\frac{G_F}{\sqrt{2}} g_{\alpha;{\rm V}}\boldsymbol{L}\phi_+^\dagger\boldsymbol{\Sigma}\phi_+\,. \tag{A.8}$$

JHEP10(2023)021

Since the spatial contribution $\boldsymbol{L}$ can be approximately neglected compared to the temporal contribution L^0, the terms with the spatial contribution will not be included in the leading order Lagrangian. The axial part can also be neglected compared to the vector part at the leading order.

As a result, the effective Lagrangian of EνES can be written with only the vector contribution as

$$\mathcal{L}_{\mathrm{E}\nu\mathrm{ES}} = -i\sqrt{2}G_F g_{\alpha;\mathrm{V}}\bar{\nu}_{\alpha,L}\gamma^0\nu_{\alpha,L}\phi_+^\dagger\phi_+ \,. \tag{A.9}$$

Open Access. This article is distributed under the terms of the Creative Commons Attribution License (CC-BY 4.0), which permits any use, distribution and reproduction in any medium, provided the original author(s) and source are credited.

JHEP10(2023)021

References

[1] J.A. Formaggio and G.P. Zeller, *From eV to EeV: neutrino cross sections across energy scales*, *Rev. Mod. Phys.* **84** (2012) 1307 [arXiv:1305.7513] [INSPIRE].

[2] KAMIOKANDE-II collaboration, *Observation of ^{8}B solar neutrinos in the Kamiokande-II detector*, *Phys. Rev. Lett.* **63** (1989) 16 [INSPIRE].

[3] SUPER-KAMIOKANDE collaboration, *Measurements of the solar neutrino flux from Super-Kamiokande's first* 300 *days*, *Phys. Rev. Lett.* **81** (1998) 1158 [*Erratum ibid.* **81** (1998) 4279] [hep-ex/9805021] [INSPIRE].

[4] BOREXINO collaboration, *First real time detection of ^{7}Be solar neutrinos by Borexino*, *Phys. Lett. B* **658** (2008) 101 [arXiv:0708.2251] [INSPIRE].

[5] C. Amsler et al., *A new measurement of the $\bar{\nu}_e e^-$ elastic cross-section at very low energy*, *Phys. Lett. B* **545** (2002) 57 [INSPIRE].

[6] TEXONO collaboration, *Limit on the electron neutrino magnetic moment from the Kuo-Sheng reactor neutrino experiment*, *Phys. Rev. Lett.* **90** (2003) 131802 [hep-ex/0212003] [INSPIRE].

[7] A.G. Beda et al., *First result for neutrino magnetic moment from measurements with the GEMMA spectrometer*, *Phys. Atom. Nucl.* **70** (2007) 1873 [arXiv:0705.4576] [INSPIRE].

[8] CHARM collaboration, *Experimental results on neutrino-electron scattering*, *Z. Phys. C* **41** (1989) 567 [*Erratum ibid.* **51** (1991) 142] [INSPIRE].

[9] LSND collaboration, *Measurement of electron-neutrino-electron elastic scattering*, *Phys. Rev. D* **63** (2001) 112001 [hep-ex/0101039] [INSPIRE].

[10] SENSEI collaboration, *SENSEI: direct-detection results on sub-GeV dark matter from a new skipper-CCD*, *Phys. Rev. Lett.* **125** (2020) 171802 [arXiv:2004.11378] [INSPIRE].

[11] EDELWEISS collaboration, *First germanium-based constraints on sub-MeV dark matter with the EDELWEISS experiment*, *Phys. Rev. Lett.* **125** (2020) 141301 [arXiv:2003.01046] [INSPIRE].

[12] SUPERCDMS collaboration, *Results from the super cryogenic dark matter search experiment at Soudan*, *Phys. Rev. Lett.* **120** (2018) 061802 [arXiv:1708.08869] [INSPIRE].

[13] K. Fujikawa and R. Shrock, *The magnetic moment of a massive neutrino and neutrino spin rotation*, *Phys. Rev. Lett.* **45** (1980) 963 [INSPIRE].

[14] C. Giunti and A. Studenikin, *Neutrino electromagnetic interactions: a window to new physics*, *Rev. Mod. Phys.* **87** (2015) 531 [arXiv:1403.6344] [INSPIRE].

[15] N.F. Bell et al., *Model independent bounds on magnetic moments of Majorana neutrinos*, *Phys. Lett. B* **642** (2006) 377 [hep-ph/0606248] [INSPIRE].

[16] N.F. Bell et al., *How magnetic is the Dirac neutrino?*, *Phys. Rev. Lett.* **95** (2005) 151802 [hep-ph/0504134] [INSPIRE].

[17] N. Viaux et al., *Neutrino and axion bounds from the globular cluster M5 (NGC 5904)*, *Phys. Rev. Lett.* **111** (2013) 231301 [arXiv:1311.1669] [INSPIRE].

[18] A.H. Córsico et al., *Constraining the neutrino magnetic dipole moment from white dwarf pulsations*, *JCAP* **08** (2014) 054 [arXiv:1406.6034] [INSPIRE].

[19] P. Carenza et al., *Strong cosmological constraints on the neutrino magnetic moment*, arXiv:2211.10432 [INSPIRE].

[20] S.-P. Li and X.-J. Xu, *Neutrino magnetic moments meet precision $N_{\rm eff}$ measurements*, *JHEP* **02** (2023) 085 [arXiv:2211.04669] [INSPIRE].

[21] XENON collaboration, *Search for new physics in electronic recoil data from XENONnT*, *Phys. Rev. Lett.* **129** (2022) 161805 [arXiv:2207.11330] [INSPIRE].

[22] N. Kurinsky, D. Baxter, Y. Kahn and G. Krnjaic, *Dark matter interpretation of excesses in multiple direct detection experiments*, *Phys. Rev. D* **102** (2020) 015017 [arXiv:2002.06937] [INSPIRE].

[23] J. Kozaczuk and T. Lin, *Plasmon production from dark matter scattering*, *Phys. Rev. D* **101** (2020) 123012 [arXiv:2003.12077] [INSPIRE].

[24] M.J. Dolan, F. Kahlhoefer and C. McCabe, *Directly detecting sub-GeV dark matter with electrons from nuclear scattering*, *Phys. Rev. Lett.* **121** (2018) 101801 [arXiv:1711.09906] [INSPIRE].

[25] D. Baxter, Y. Kahn and G. Krnjaic, *Electron ionization via dark matter-electron scattering and the Migdal effect*, *Phys. Rev. D* **101** (2020) 076014 [arXiv:1908.00012] [INSPIRE].

[26] G.B. Gelmini, V. Takhistov and E. Vitagliano, *Scalar direct detection: in-medium effects*, *Phys. Lett. B* **809** (2020) 135779 [arXiv:2006.13909] [INSPIRE].

[27] Z.-L. Liang, C. Mo, F. Zheng and P. Zhang, *Describing the Migdal effect with a bremsstrahlung-like process and many-body effects*, *Phys. Rev. D* **104** (2021) 056009 [arXiv:2011.13352] [INSPIRE].

[28] Y. Hochberg et al., *Determining dark-matter-electron scattering rates from the dielectric function*, *Phys. Rev. Lett.* **127** (2021) 151802 [arXiv:2101.08263] [INSPIRE].

[29] S. Knapen, J. Kozaczuk and T. Lin, *Dark matter-electron scattering in dielectrics*, *Phys. Rev. D* **104** (2021) 015031 [arXiv:2101.08275] [INSPIRE].

[30] Z.-L. Liang, C. Mo and P. Zhang, *In-medium screening effects for the galactic halo and solar-reflected dark matter detection in semiconductor targets*, *Phys. Rev. D* **104** (2021) 096001 [arXiv:2107.01209] [INSPIRE].

[31] A. Mitridate, T. Trickle, Z. Zhang and K.M. Zurek, *Dark matter absorption via electronic excitations*, *JHEP* **09** (2021) 123 [arXiv:2106.12586] [INSPIRE].

JHEP10(2023)021

[32] R. Penco, *An introduction to effective field theories*, arXiv:2006.16285 [INSPIRE].

[33] I.Z. Rothstein, *TASI lectures on effective field theories*, hep-ph/0308266 [INSPIRE].

[34] D.W. Snoke, *Solid state physics*, Cambridge University Press, Cambridge, U.K. (2020) [DOI:10.1017/9781108123815].

[35] S. Knapen, J. Kozaczuk and T. Lin, *Python package for dark matter scattering in dielectric targets*, *Phys. Rev. D* **105** (2022) 015014 [arXiv:2104.12786] [INSPIRE].

[36] S. Knapen, J. Kozaczuk and T. Lin, *Dark matter-electron scattering in dielectrics*, *Phys. Rev. D* **104** (2021) 015031 [arXiv:2101.08275] [INSPIRE].

[37] J.N. Bahcall and A.M. Serenelli, *How do uncertainties in the surface chemical abundances of the sun affect the predicted solar neutrino fluxes?*, *Astrophys. J.* **626** (2005) 530 [astro-ph/0412096] [INSPIRE].

[38] J.N. Bahcall, A.M. Serenelli and S. Basu, *New solar opacities, abundances, helioseismology, and neutrino fluxes*, *Astrophys. J. Lett.* **621** (2005) L85 [astro-ph/0412440] [INSPIRE].

[39] R. Essig, M. Sholapurkar and T.-T. Yu, *Solar neutrinos as a signal and background in direct-detection experiments searching for sub-GeV dark matter with electron recoils*, *Phys. Rev. D* **97** (2018) 095029 [arXiv:1801.10159] [INSPIRE].

[40] M. Atzori Corona et al., *New constraint on neutrino magnetic moment and neutrino millicharge from LUX-ZEPLIN dark matter search results*, *Phys. Rev. D* **107** (2023) 053001 [arXiv:2207.05036] [INSPIRE].

[41] XENON collaboration, *Excess electronic recoil events in XENON1T*, *Phys. Rev. D* **102** (2020) 072004 [arXiv:2006.09721] [INSPIRE].

[42] SuperCDMS collaboration, *Projected sensitivity of the SuperCDMS SNOLAB experiment*, *Phys. Rev. D* **95** (2017) 082002 [arXiv:1610.00006] [INSPIRE].

[43] B. Yue, J. Liao and J. Ling, *Probing neutrino magnetic moment at the Jinping neutrino experiment*, *JHEP* **08** (2021) 068 [arXiv:2102.12259] [INSPIRE].

[44] EDELWEISS collaboration, *Sub-GeV dark matter searches with EDELWEISS: new results and prospects*, *SciPost Phys. Proc.* **12** (2023) 012 [arXiv:2211.04176] [INSPIRE].

JHEP10(2023)021